

iScheduler: Reinforcement Learning–Driven Continual Optimization for Large-Scale Resource Investment Problems

Yi-Xiang Hu*, Yuke Wang*, Feng Wu†, Zirui Huang, Shuli Zeng, Xiang-Yang Li†

School of Computer Science and Technology, University of Science and Technology of China
 {yixianghu,yk.wang,hzr090901,zengshuli0130}@mail.ustc.edu.cn, {wufeng02,xiangyangli}@ustc.edu.cn

Abstract

Scheduling precedence-constrained tasks under shared renewable resources is central to modern computing platforms. The Resource Investment Problem (RIP) models this setting by minimizing the cost of provisioned renewable resources under precedence and timing constraints. Exact mixed-integer programming and constraint programming become impractically slow on large instances, and dynamic updates require schedule revisions under tight latency budgets. We present iScheduler, a reinforcement-learning-driven iterative scheduling framework that formulates RIP solving as a Markov decision process over decomposed subproblems and constructs schedules through sequential process selection. The framework accelerates optimization and supports reconfiguration by reusing unchanged process schedules and rescheduling only affected processes. We also release L-RIPLIB, an industrial-scale benchmark derived from cloud-platform workloads with 1,000 instances of 2,500–10,000 tasks. Experiments show that iScheduler attains competitive resource costs while reducing time to feasibility by up to 43× against strong commercial baselines.

1 Introduction

Scheduling precedence-constrained tasks under limited shared resources (e.g., GPUs or network bandwidth) is fundamental to modern computing platforms (Liu et al. 2024; Si et al. 2026). In production settings, task parameters rarely remain static: execution durations, feasible time windows, and resource requirements shift with workload demand, system congestion, and unexpected delays (Cai, Bian, and Liu 2024; Teichtel-Königsbuch et al. 2023; Li et al. 2022). Each fluctuation triggers a *reconfiguration request* that must be handled under tight latency budgets. This makes fast schedule adaptation both essential and difficult.

These scheduling settings are commonly formalized as Resource Investment Problems (RIPs), where the objective is to minimize the cost of allocating renewable resources while satisfying precedence and timing requirements (Stefan et al. 2018). RIPs are known to be NP-complete (Ganian, Hamm, and Mescoff 2021), and mainstream approaches rely on Mixed Integer Programming (MIP) or Constraint Programming (CP). However, these solvers incur prohibitive

runtimes on large instances. For example, a 10,000-task project with millions of decision variables can require hours of computation even with a strong commercial solver (e.g., Gurobi) (Gurobi Optimization, LLC 2025). This leads to our first challenge: (C1) *How to generate high-quality schedules for large RIP instances within practical computation limits?*

A standard strategy for scaling to large instances is iterative decomposition, which partitions the instance into smaller subproblems solved across multiple rounds (Debels and Vanhoucke 2007; Li and Willis 1992; Liu, Xu, and Li 2021; Subramanya et al. 2025). However, we observe that the *order* in which tasks or task groups are scheduled strongly influences the final solution quality (see Section 3.3). Heuristic selection rules (e.g., critical-path, slack-based rules, or resource-profile heuristics) exhibit large performance variation across instances. This leads to our second challenge: (C2) *How to select scheduling orders that outperform fixed heuristics and generalize across instances?*

Meanwhile, when task parameters change, re-solving the entire RIP from scratch is operationally unacceptable. In many deployments, only a small portion of the schedule is affected, yet traditional solvers must recompute globally. Therefore, the core dynamic-setting challenge is: (C3) *How to update schedules efficiently under parameter variations without restarting the solving process?*

To address these challenges, we propose iScheduler, a reinforcement learning–driven iterative scheduling framework for large-scale RIPs. We decompose the project into task subsets and formulate the iterative scheduling process as a Markov Decision Process (MDP). The agent learns a value function that captures long-range interactions induced by shared resources and overlapping time windows, enabling effective selection of the next subset to schedule (addresses C1 and C2). During reconfiguration, iScheduler schedules only the impacted portions while retaining unchanged schedules, which sharply reduces recomputation (addresses C3). We also introduce L-RIPLIB, an industrial-scale RIP benchmark derived from cloud computing workloads. It contains 1,000 instances ranging from 2,500 to 10,000 tasks, serving as a large-scale complement to PSPLIB (Kolisch and Sprecher 1997).

Our contributions are threefold:

- **iScheduler Framework.** We formulate large-scale RIP solving as a sequential decision process over decom-

*These authors contributed equally.

†Corresponding authors.

posed subproblems and learn adaptive process-selection policies that account for long-range interactions induced by shared resources and overlapping time windows. The same framework supports reconfiguration by reusing unchanged process schedules and rescheduling only affected processes.

- **L-RIPLIB Benchmark.** We release an industrial-scale RIP dataset with 1,000 instances and up to 10,000 tasks per instance, designed to evaluate large-scale optimization and reconfiguration settings beyond PSPLIB.
- **Empirical Results.** On L-RIPLIB, iScheduler matches competitive resource costs while reducing time to feasibility by up to $43\times$ against strong commercial baselines. Under dynamic updates, it achieves lower reconfiguration latency and stronger solution quality than state-of-the-art baselines.

2 Related Work

2.1 Resource Investment Problem

The RIP considers a set of non-preemptive tasks T , each with execution time and renewable resource demands. Tasks satisfy precedence constraints, and the objective assigns start times to ensure completion within the prescribed duration while minimizing the total cost of provisioned resources.

Formally, an RIP instance is defined as $q = \langle T, \mathcal{R}, P, r, c, d, e, l \rangle$. Let \mathcal{R} denote the set of renewable resources. Provisioning one unit of resource $k \in \mathcal{R}$ incurs cost c_k , and R_k denotes the amount of resource k provisioned for the entire project. Each task $i \in T$ requires $r_{i,k}$ units of resource k during its duration d_i . Precedence relations are $P \subseteq T \times T$. Tasks also have earliest start times e_i and deadlines l_i . A schedule assigns each task i a start time S_i . The consumption of resource k at time t is $\sum_{i \in \mathcal{U}(S,t)} r_{i,k}$, where $\mathcal{U}(S,t)$ is the set of tasks active at time t .

The RIP can be formulated as:

$$\min \sum_{k \in \mathcal{R}} c_k R_k \quad (1)$$

$$\text{s.t. } S_i + d_i \leq S_j \quad \forall (i, j) \in P, \quad (2)$$

$$\sum_{i \in \mathcal{U}(S,t)} r_{i,k} \leq R_k \quad \forall k \in \mathcal{R}, \forall t, \quad (3)$$

$$e_i \leq S_i \leq l_i - d_i \quad \forall i \in T, \quad (4)$$

$$R_k \geq 0 \quad \forall k \in \mathcal{R}. \quad (5)$$

Reconfiguration. In deployments, task durations, resource demands, and precedence relations vary due to workload shifts or operational adjustments. Let $q = \langle T, \mathcal{R}, P, r, c, d, e, l \rangle$, $q' = \langle T', \mathcal{R}, P', r', c, d', e', l' \rangle$ denote the original and updated instances. *Classical optimization* ($h(q') \rightarrow (S_i)_{i \in T'}$) solves q' independently, discarding prior computation. *Continual optimization* ($f(q, (S_i)_{i \in T}, q') \rightarrow (S_i)_{i \in T'}$) instead seeks a solution update, that reuses the previous schedule to reduce recomputation while preserving solution quality.

2.2 Traditional RIP Benchmarks

The most widely used dataset for RIP research is PSPLIB (Kolisch and Sprecher 1997), generated via Pro-

Gen (Kolisch, Sprecher, and Drexl 1995). This dataset contains 2040 project instances, ranging from 30 to 120 activities, with optimal solutions available for each instance. Additionally, the RG30 and RG300 datasets, introduced by (Vanhoucke et al. 2008) and generated by the RanGen (De-meulemeester, Vanhoucke, and Herroelen 2003), include 2280 instances with 30 to 300 activities. A comprehensive summary of these datasets is provided by (Vanhoucke, Coelho, and Batselier 2016). RIPLib (Gerhards 2020) offers 4950 multi-mode RIP instances with 30–100 activities. These datasets emphasize small instances (typically fewer than 500 tasks), limiting relevance to industrial-scale problems.

2.3 Scalability Challenge

Large RIP instances produce mathematical programs with millions of variables and strong temporal coupling among tasks. Direct MIP or CP solving becomes impractical when $|T|$ reaches thousands. Recent work scales via decomposition. The Partitioned Optimization Problem (POP) framework (Narayanan et al. 2021) partitions resource allocation problems into independent subproblems and merges their solutions. POP achieves substantial speedups when dependencies are weak and resource usage is granular. However, RIP violates these assumptions: precedence constraints and time-dependent resource profiles create cross-partition dependencies that prevent naive decomposition. COpt (Subramanya et al. 2025) adopts a continual re-optimization workflow, reusing prior solutions as warm-starts to accelerate recomputation when system conditions shift.

3 iScheduler Framework

This section presents the iScheduler framework (Figure 1). The core idea is to solve a large-scale RIP through an iterative decomposition workflow: we decompose the task set into processes, build a process-level interaction graph, and then use reinforcement learning (RL) to decide which process to schedule next at each iteration. Each iteration constructs and solves one subproblem, commits one local schedule, and updates the global resource-usage profile and the process-level state until all processes have been scheduled.

3.1 Decomposition

We start from the task-level directed acyclic graph (DAG) $G_T = (T, P)$, where each node is a task and each directed edge $(i, j) \in P$ denotes a precedence constraint requiring i to finish before j starts. We group tasks into processes by taking the weakly connected components of G_T . Concretely, each process \mathcal{P}_i corresponds to one weakly connected component of the task DAG when ignoring edge directions. This choice yields cohesive groups whose precedence relations live largely inside the same group, so a process forms a natural scheduling unit for iterative solving. Let $T_{\mathcal{P}_i} \subseteq T$ denote the set of tasks that belong to process \mathcal{P}_i .

After defining processes, iScheduler builds a process-level graph $G_{PL} = (V_{PL}, E_{PL})$ to represent interactions among processes. An undirected edge $(\mathcal{P}_i, \mathcal{P}_j) \in E_{PL}$ exists when tasks in the two processes have overlapping feasi-

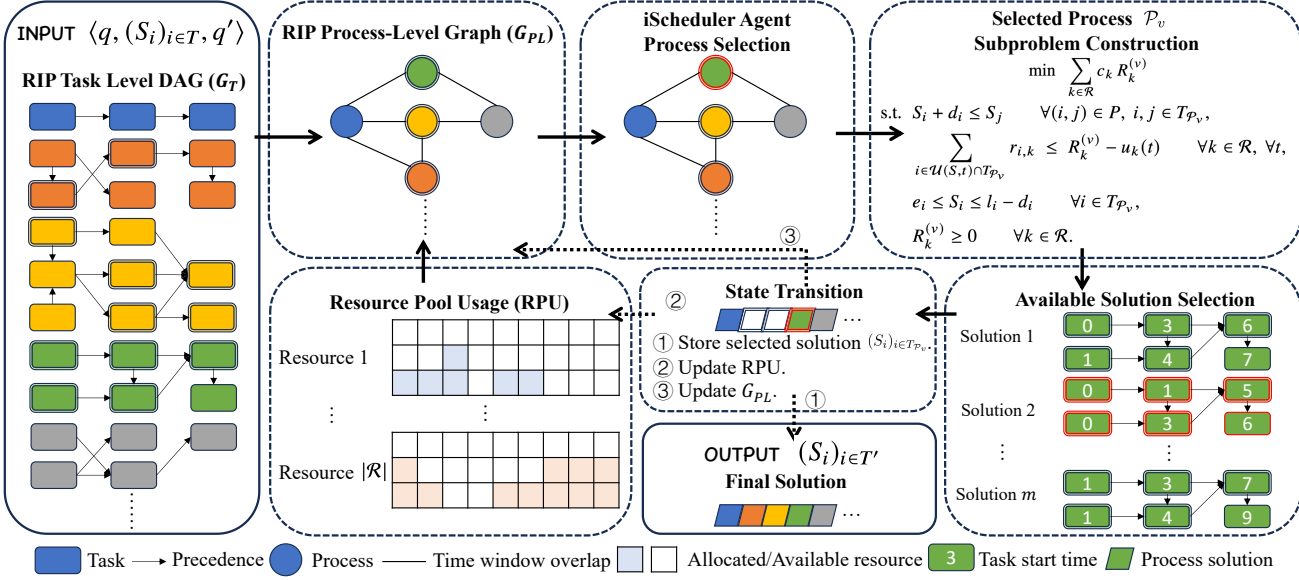


Figure 1: Overview of the iScheduler framework. (1) The RIP is first represented as a task-level DAG (G_T), where nodes represent tasks and edges denote precedence constraints. Tasks are grouped into processes by taking the weakly connected components of G_T (ignoring edge directions). A process-level graph G_{PL} is then constructed over these processes, where an edge indicates overlapping feasible time windows (potential resource contention). (2) At each iteration, the iScheduler agent observes the current scheduling state and Resource Pool Usage ($RPU = \{u_k(t)\}_{k \in \mathcal{R}}$), and selects an unscheduled process \mathcal{P}_v from G_{PL} . (3) A subproblem RIP _{v} is constructed and solved to generate multiple candidate schedules for tasks in $T_{\mathcal{P}_v}$, from which one solution is selected and committed. (4) The committed start times ($S_i|_{i \in T_{\mathcal{P}_v}}$, G_{PL} , and RPU are updated accordingly. This iterative procedure continues until all processes in G_{PL} have been scheduled, resulting in the final schedule. **Double-bordered nodes** indicate tasks or processes with changed parameters (i.e., reconfiguration requests), and **red** highlights the currently selected process or solution during scheduling.

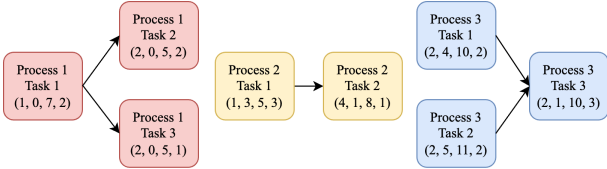


Figure 2: Task structures of three processes in an RIP. Each block represents a task, annotated as $(d_i, e_i, l_i, r_{i,1})$, where d_i is the duration, e_i the earliest start time, l_i the deadline, and $r_{i,1}$ the demand for resource 1. Directed arrows denote precedence constraints: a task must finish before any successor can start.

ble time windows:

$$[e_u, l_u] \cap [e_v, l_v] \neq \emptyset, \quad u \in T_{\mathcal{P}_i}, v \in T_{\mathcal{P}_j}.$$

In RIP, renewable resources are constrained at each time t by a global capacity, so coupling across groups arises only through possible temporal concurrency. If two processes contain tasks whose feasible windows overlap, then there exists at least one feasible time interval where tasks from both processes could be active, and their resource demands then compete against the same resource pool. As a result, committing a schedule for one process reduces the feasible region of the other through the shared resource constraint. This

is why G_{PL} uses window overlap to encode inter-process contention.

Resource contention requires potential simultaneity; the overlap condition is exactly the criterion that rules in potential simultaneity across processes, and all downstream contention intensity is carried by the edge features and the evolving resource-usage profile defined later.

3.2 Subproblem Construction

Under reconfiguration, only processes whose task parameters changed are marked “unscheduled”; the remaining processes keep their previously committed schedules. This restricts recomputation to the affected region.

Let $u_k(t)$ denote the current Resource Pool Usage (RPU) for resource $k \in \mathcal{R}$ at time t induced by already scheduled processes. We denote the full usage profile by $RPU = \{u_k(t)\}_{k \in \mathcal{R}}$.

At iteration v , iScheduler selects one unscheduled process \mathcal{P}_v and schedules tasks in $T_{\mathcal{P}_v}$, treating previously scheduled tasks as fixed. The resulting subproblem RIP _{v} takes the same RIP structure but uses the remaining resource budget ($R_k^{(v)} - u_k(t)$) inside the resource constraints ($R_k^{(v)}$ denotes

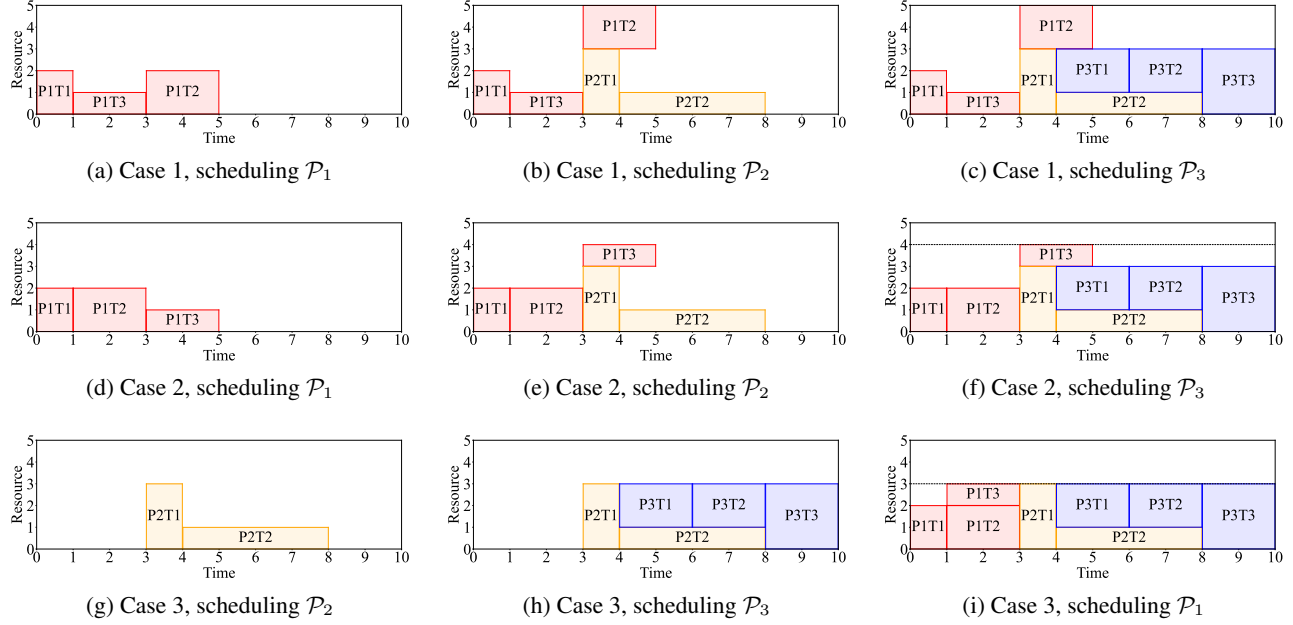


Figure 3: Effect of scheduling order and local solution selection on final performance. Each \mathcal{P}_i denotes a process, and each task in a process is labeled as $P_i T_j$, where i indexes the process and j indexes the task within that process. Different scheduling orders and local schedule choices lead to different resource usage outcomes. Case 1: Scheduling $\mathcal{P}_1 \rightarrow \mathcal{P}_2 \rightarrow \mathcal{P}_3$ results in total resource usage $R_1 = 5$. Case 2: Using the *same* scheduling order but selecting an alternative local solution for \mathcal{P}_2 yields $R_1 = 4$. Case 3: Changing the scheduling order to $\mathcal{P}_2 \rightarrow \mathcal{P}_3 \rightarrow \mathcal{P}_1$ further reduces usage to $R_1 = 3$.

the global provisioned capacity after iteration v):

$$\min \sum_{k \in \mathcal{R}} c_k R_k^{(v)} \quad (6)$$

$$\text{s.t. } S_i + d_i \leq S_j \quad \forall (i, j) \in P, i, j \in T_{\mathcal{P}_v}, \quad (7)$$

$$\sum_{i \in \mathcal{U}(S, t) \cap T_{\mathcal{P}_v}} r_{i,k} \leq R_k^{(v)} - u_k(t) \quad \forall k \in \mathcal{R}, \forall t, \quad (8)$$

$$e_i \leq S_i \leq l_i - d_i \quad \forall i \in T_{\mathcal{P}_v}, \quad (9)$$

$$R_k^{(v)} \geq 0 \quad \forall k \in \mathcal{R}. \quad (10)$$

Solving RIP_v yields start times $(S_i)_{i \in T_{\mathcal{P}_v}}$, after which iScheduler updates the global usage profile $u_k(t)$ and removes \mathcal{P}_v from the unscheduled set. The procedure terminates when all unscheduled processes are resolved, and the final schedule aggregates newly optimized processes with retained unchanged ones.

To quantify the impact of decomposition on problem size, consider an instance with $|T| = 10,000$ tasks. The original monolithic formulation yields a global optimization problem with 3,706,353 variables and 43,701 constraints. Decomposition splits the instance into 330 processes, and the resulting subproblems contain 3,748.5 variables and 1,482.7 constraints on average. This reduction directly shrinks the search space explored by exact solvers and strengthens per-subproblem propagation, since fewer decision variables, tighter local precedence structure, and shorter interacting time horizons reduce the depth and breadth of branching

required to reach feasibility and improve bounds. For NP-hard RIP instances, the solver workload scales sharply with problem size; the above reduction therefore translates into substantially lower optimization effort per iteration.

3.3 Why Scheduling Order Matters

Although decomposition reduces the scale of each subproblem, it introduces a critical degree of freedom: the order in which processes are scheduled. Let $\{\mathcal{P}_1, \dots, \mathcal{P}_n\}$ be the decomposed unscheduled processes. Different scheduling orders correspond to different permutations:

$$\mathcal{P}_{\pi(1)} \rightarrow \mathcal{P}_{\pi(2)} \rightarrow \dots \rightarrow \mathcal{P}_{\pi(n)},$$

where π is a permutation of indices. Since scheduling a process updates resource usage and shifts the feasible regions of remaining processes, the global solution is sensitive to this ordering. Taking the toy RIP instance in Figure 2 as an illustration, even under the same decomposition strategy, different scheduling orders or different committed local schedules can lead to different global resource costs (Figure 3):

- Case 1 and Case 2 share the same scheduling order but commit different local solutions, resulting in different overall resource costs.
- Case 1 and Case 3 use different scheduling orders, leading to further variation in utilization and feasibility.

Thus, two coupled decisions directly influence the final outcome: (1) *which process to schedule next*, and (2) *which*

local schedule to commit for that process. The combined decision space is large ($n!$ possible orders and multiple local solutions per process), and choices made early have long-term influence. This structure naturally forms a sequential decision problem, motivating an RL-based policy instead of fixed heuristics.

3.4 MDP Formulation

Following the decomposition and subproblem construction described above, the iterative scheduling procedure can be naturally modeled as an MDP $\langle \mathcal{X}, \mathcal{A}, \mathcal{T}, \mathcal{W}, \gamma \rangle$, where \mathcal{X} is the state space, \mathcal{A} is the action space, $\mathcal{T}(\mathbf{x}' \mid \mathbf{x}, a)$ is the transition function, $\mathcal{W}(\mathbf{x}, a, \mathbf{x}')$ is the reward function, and $\gamma \in (0, 1)$ is the discount factor.

State Space \mathcal{X} . A state \mathbf{x} summarizes all relevant information of the current solving iteration. After decomposition, each RIP instance is represented by a process-level graph G_{PL} with node and edge features, together with the current RPU. Specifically, each process node is annotated with 4 node features, and each edge with 5 relational features (Section 3.5). An example of such a state representation is shown in Figure 4. Thus, the state space \mathcal{X} consists of all annotated graphs arising from partially scheduled RIP instances, motivating the use of a GNN-based Q-network as the value function approximator.

Action Space \mathcal{A} . At each iteration, the agent selects one process from the unscheduled candidate set $\mathcal{C}_{PL} \subseteq G_{PL}$, $\mathcal{A}(\mathbf{x}) = \mathcal{C}_{PL}$. As illustrated by the green nodes in Figure 4, each action corresponds to selecting a process \mathcal{P}_v to schedule next. Given the current state \mathbf{x} , the Q-network outputs $Q(\mathbf{x}, \mathcal{P}_v)$ for all $\mathcal{P}_v \in \mathcal{A}(\mathbf{x})$.

Transition Function \mathcal{T} . Transitions in this environment are deterministic. When the agent selects a process \mathcal{P}_v at iteration v , the solver (i) constructs its subproblem based on the task set $T_{\mathcal{P}_v}$ and current resource usage, (ii) commits one local schedule, (iii) updates the RPU and all node/edge features, and (iv) removes \mathcal{P}_v from the candidate set. This results in the next state \mathbf{x}_{v+1} . Therefore, $\mathcal{T}(\mathbf{x}_{v+1} \mid \mathbf{x}_v, \mathcal{P}_v) = 1$. Figure 4 illustrates such a transition, where selecting \mathcal{P}_1 changes its status and updates the associated features.

Reward Function \mathcal{W} . The goal of the agent is to minimize the final resource cost of the complete schedule. Since intermediate iterations do not correspond to meaningful costs, rewards are given only upon completion. For an action \mathcal{P}_v taken at state \mathbf{x}_v , the reward is defined as:

$$\mathcal{W}(\mathbf{x}_v, \mathcal{P}_v, \mathbf{x}_{v+1}) = \alpha \cdot \mathbb{I}(\text{all processes scheduled}) \cdot \left(\frac{OPT}{Obj} \right), \quad (11)$$

where Obj is the objective value (total resource cost) of the final schedule, OPT is a time-capped lower bound obtained via a CP solver, and $\alpha > 0$ is a scaling factor. This final-step reward encourages the agent to search for global scheduling orders that achieve low-cost solutions rather than optimizing local intermediate decisions.

3.5 State Feature Representation

This section describes the node and edge features used to construct the graph-structured state $\mathbf{x} \in \mathcal{X}$ within the MDP.

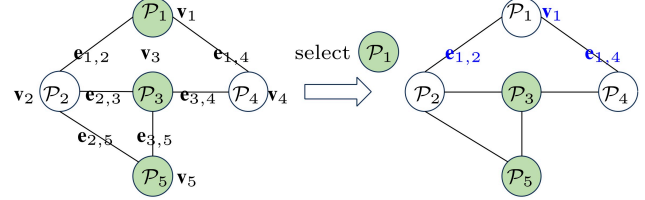


Figure 4: State transition: When one of the three considered action nodes (in green) is selected, it transitions to a new state and updates the associated features (in blue).

These features encode structural, temporal, and resource-related information of each process and its interactions, and are embedded using a Graph Neural Network (GNN) for learning the process selection policy.

Process Node Features. Each node corresponds to a process \mathcal{P} with task set $T_{\mathcal{P}}$. We extract four node features: 1) Minimum internal processing time. The intrinsic processing time (analogous to makespan) of process \mathcal{P} : $PT_{\mathcal{P}} = \sum_{i \in T_{\mathcal{P}}} d_i$. 2) Average weighted resource demand. A normalized measure of the resource requirements within \mathcal{P} :

$$\text{WRD}_{\mathcal{P}} = \frac{1}{|T_{\mathcal{P}}| \sum_{k \in \mathcal{R}} c_k} \sum_{i \in T_{\mathcal{P}}} \sum_{k \in \mathcal{R}} c_k r_{i,k}.$$

3) Scheduling order encoding. If \mathcal{P} has been scheduled, its node stores the corresponding scheduling iteration index; otherwise, the value is 0. 4) Weighted resource usage in feasible window. Using the global resource usage profile $u_k(t)$:

$$\text{WRU}_{\mathcal{P}}(ES_{\mathcal{P}}, LF_{\mathcal{P}}) = \frac{1}{\sum_{k \in \mathcal{R}} c_k} \sum_{k \in \mathcal{R}} \frac{c_k}{R_k} \sum_{t=ES_{\mathcal{P}}}^{LF_{\mathcal{P}}} u_k(t),$$

where $ES_{\mathcal{P}} = \min_{i \in T_{\mathcal{P}}} e_i$ and $LF_{\mathcal{P}} = \max_{i \in T_{\mathcal{P}}} l_i$.

Relation Edge Features. For each edge $(\mathcal{P}_i, \mathcal{P}_j) \in G_{PL}$, we compute five edge features: 1) Start and end of overlap window: $t_{\text{start}} = \max(ES_{\mathcal{P}_i}, ES_{\mathcal{P}_j})$, $t_{\text{end}} = \min(LF_{\mathcal{P}_i}, LF_{\mathcal{P}_j})$. 2) Ratio of shared resource types: $\frac{|\mathcal{R}_{\mathcal{P}_i} \cap \mathcal{R}_{\mathcal{P}_j}|}{|\mathcal{R}|}$, where $\mathcal{R}_{\mathcal{P}}$ is the set of resource types required by tasks in \mathcal{P} . 3) Weighted resource usage of \mathcal{P}_i and \mathcal{P}_j in the overlap window: $\text{WRU}_{\mathcal{P}_i}(t_{\text{start}}, t_{\text{end}})$ and $\text{WRU}_{\mathcal{P}_j}(t_{\text{start}}, t_{\text{end}})$. 4) Combined weighted utilization of both processes. 5) Normalized system-wide resource utilization in the same window. These edge features quantify how two processes compete for resources and how their scheduling may interfere with one another.

GNN Architecture. We adopt the GATv2 (Brody, Alon, and Yahav 2021), implemented using PyTorch-Geometric (Fey and Lenssen 2019). Each message-passing layer updates node embeddings while preserving graph topology. Let \mathbf{v}_i denote the feature vector of process node i , and let $\mathbf{e}_{i,j}$ denote the edge feature between nodes i and j . Each layer performs the update:

$$\mathbf{v}'_i = \sum_{j \in \mathcal{N}(i) \cup \{i\}} \beta_{i,j} \Theta_a \mathbf{v}_j, \quad (12)$$

Algorithm 1: Continual Optimization Interface $f(q, (S_i)_{i \in T}, q') \rightarrow (S_i)_{i \in T'}$ (iScheduler Execution, Reconfiguration-Aware)

Input: Original RIP instance $q = \langle T, \mathcal{R}, P, r, c, d, e, l \rangle$, previous schedule $(S_i)_{i \in T}$, updated instance $q' = \langle T', \mathcal{R}, P', r', c, d', e', l' \rangle$, trained iScheduler agent with Q-function Q and value network F_ϕ
Output: Updated schedule $(S_i)_{i \in T'}$

```

1:  $v \leftarrow 0$  ▷ Iteration counter
2:  $(G_{PL}, (u_k)_{k \in \mathcal{R}}, \mathcal{C}_{PL}) \leftarrow$   

   InitializeReconfig( $q, (S_i)_{i \in T}, q'$ ) ▷ Build  $G_{PL}$  for  $q'$   
and reuse unchanged schedules
3: Initialize any bookkeeping for task-level schedule on  $T'$ 
4: while  $\mathcal{C}_{PL} \neq \emptyset$  do
5:    $x_v \leftarrow \text{MDP}(G_{PL}, (u_k)_{k \in \mathcal{R}}, \mathcal{C}_{PL})$ 
6:    $\mathcal{P}_v \leftarrow \arg \max_{\mathcal{P} \in \mathcal{C}_{PL}} Q(x_v, \mathcal{P})$ 
7:    $\text{RIP}_v \leftarrow \text{Subproblem}(\mathcal{P}_v, (u_k)_{k \in \mathcal{R}})$ 
8:   Solve  $\text{RIP}_v$  to obtain  $m$  local solutions  $\{A_{j,v}\}_{j=1}^m$ 
9:   Compute scores  $s_{j,v} \leftarrow F_\phi(x_v, A_{j,v})$  for  $j = 1, \dots, m$ 
10:   $j^* \leftarrow \arg \min_j s_{j,v}$ , commit  $A_{j^*,v}$  to update  $(u_k)_{k \in \mathcal{R}}$  and the schedule of tasks in  $T_{\mathcal{P}_v}$ 
11:  Remove  $\mathcal{P}_v$  from  $\mathcal{C}_{PL}$ 
12:  Update  $G_{PL}$  using  $(u_k)_{k \in \mathcal{R}}$ 
13:   $v \leftarrow v + 1$ 
14: end while
15: Aggregate per-process schedules (including unchanged processes) to obtain  $(S_i)_{i \in T'}$ 
16: return Updated schedule  $(S_i)_{i \in T'}$ 

```

where $\mathcal{N}(i)$ is the neighborhood of i in the process-level graph. The attention coefficients $\beta_{i,j}$ are computed as:

$$\beta_{i,j} = \text{softmax}(\mathbf{a}^\top \text{LeakyReLU}(\Theta_b \mathbf{v}_i + \Theta_a \mathbf{v}_j + \Theta_e \mathbf{e}_{i,j})) , \quad (13)$$

where Θ_a , Θ_b , Θ_e and \mathbf{a} are trainable parameters. Each GNN layer has its own parameter set, enabling hierarchical aggregation of relational information across processes.

3.6 Learning-Based Solution Selection

We augment iScheduler with a learning-based solution-selection module that predicts the global effect of each candidate schedule.

At iteration v , given the current state x_v and a set of m candidate solutions $\{A_{1,v}, \dots, A_{m,v}\}$ for process P_v , we introduce a value network $F_\phi(x_v, A_{j,v})$ that estimates the final objective value when committing solution $A_{j,v}$ at this step. The selected solution is then $A_{j^*,v}$, where $j^* = \arg \min_j F_\phi(x_v, A_{j,v})$.

Feature design. We reuse the process-level graph representation and RPU as the global state features. A GNN encoder produces a global embedding h_v by aggregating node and edge features over the process-level graph. For each candidate solution $A_{j,v}$, we compute a feature vector $z_{j,v}$ that summarizes its local impact, including (i) incremental resource-usage statistics (e.g., RMS, total variation, peak utilization and its time position), (ii) overlap between its

Algorithm 2: iScheduler Training (Reconfiguration-Aware DQN)

Input: Training triples $\{(q_i, (S_i)_{i \in T_i}, q'_i)\}_{i=1}^M$, scaling factor α , minibatch size k , learning rate lr , replay buffer size N , discount factor γ , exploration probability ϵ , target update frequency K , solution pool size m
Output: Q-function approximator \hat{Q}^* (trained RL agent)

```

1: Initialize replay memory  $\mathcal{H}$  to capacity  $N$ 
2: Initialize online Q-network  $\hat{Q}$  with parameters  $\theta$ 
3: Initialize target network  $\hat{Q}^*$  with  $\theta^- \leftarrow \theta$ 
4: for  $i = 1$  to  $M$  do ▷ Solve each reconfiguration instance
5:    $v \leftarrow 0$ 
6:    $(G_{PL}, (u_k)_{k \in \mathcal{R}}, \mathcal{C}_{PL}) \leftarrow$   

   InitializeReconfig( $q_i, (S_i)_{i \in T_i}, q'_i$ ) ▷ Initialize  $G_{PL}$  for  $q'_i$ 
7:    $x_0 \leftarrow \text{MDP}(G_{PL}, (u_k)_{k \in \mathcal{R}}, \mathcal{C}_{PL})$ 
8:   while  $\mathcal{C}_{PL} \neq \emptyset$  do
9:     With probability  $\epsilon$  select a random action  $\mathcal{P}_v \in \mathcal{C}_{PL}$ ,  

     otherwise  $\mathcal{P}_v \leftarrow \arg \max_{\mathcal{P} \in \mathcal{C}_{PL}} \hat{Q}(x_v, \mathcal{P})$ 
10:     $\text{RIP}_v \leftarrow \text{Subproblem}(\mathcal{P}_v, (u_k)_{k \in \mathcal{R}})$ 
11:    Solve  $\text{RIP}_v$  to obtain  $m$  local solutions  $\{A_{j,v}\}_{j=1}^m$ 
12:    Apply  $F_\phi$  to select  $A_{j^*,v}$  and commit it to update  $(u_k)_{k \in \mathcal{R}}$  and the schedule of tasks in  $T_{\mathcal{P}_v}$ 
13:    Remove  $\mathcal{P}_v$  from  $\mathcal{C}_{PL}$  and update  $G_{PL}$ 
14:    Obtain next state  $x_{v+1} \leftarrow \text{MDP}(G_{PL}, (u_k)_{k \in \mathcal{R}}, \mathcal{C}_{PL})$ 
15:    Compute reward  $r_v \leftarrow \mathcal{W}(x_v, \mathcal{P}_v, x_{v+1})$  (final-step reward as in Eq. (11))
16:    Store transition  $(x_v, \mathcal{P}_v, r_v, x_{v+1})$  in  $\mathcal{H}$ 
17:     $v \leftarrow v + 1$ 
18:    Sample a random minibatch  $(x_j, \mathcal{P}_j, r_j, x'_j)$  from  $\mathcal{H}$ 
19:     $y_j \leftarrow \begin{cases} r_j, & \text{if } x'_j \text{ is terminal,} \\ r_j + \gamma \max_{\mathcal{P}} \hat{Q}^*(x'_j, \mathcal{P}), & \text{otherwise.} \end{cases}$ 
20:    Perform a gradient descent step on  $(y_j - \hat{Q}(x_j, \mathcal{P}_j))^2$  w.r.t.  $\theta$ 
21:    Every  $K$  steps, update target parameters:  $\theta^- \leftarrow \theta$ 
22: end while
23: end for
24: return Trained Q-function approximator  $\hat{Q}^*$ 

```

execution window and neighboring processes, and (iii) temporal slack relative to deadlines. The value network then scores each candidate via

$$s_{j,v} = F_\phi(x_v, A_{j,v}) = \text{MLP}([h_v \parallel z_{j,v}]), \quad (14)$$

where $[\cdot \parallel \cdot]$ denotes vector concatenation.

Offline training. We train F_ϕ offline from solved trajectories. For each training instance and each iteration v , we generate or enumerate multiple candidate solutions $\{A_{j,v}\}_{j=1}^m$. For each candidate, we complete the remaining scheduling procedure using a fixed baseline policy and record the resulting objective value $\text{Obj}_{j,v}$. This yields supervision tuples $(x_v, \{A_{j,v}\}_{j=1}^m, \{\text{Obj}_{j,v}\}_{j=1}^m)$. Rather than regressing the

exact objective, we employ a pairwise ranking loss that encourages the network to order candidates consistently with their final costs $\mathcal{L}_{\text{rank}}$:

$$\sum_{\text{Obj}_{j,v} < \text{Obj}_{k,v}} \log \left(1 + \exp \left(F_{\phi}(x_v, A_{j,v}) - F_{\phi}(x_v, A_{k,v}) \right) \right). \quad (15)$$

This formulation focuses on relative quality between candidates and is robust to scale differences across instances.

3.7 RL Training and Execution

We instantiate the continual-optimization interface $f(q, (S_i)_{i \in T}, q') \rightarrow (S_i)_{i \in T'}$, where q and q' denote the original and updated RIP instances. Given a previous schedule $(S_i)_{i \in T}$, execution begins by reusing schedules of unchanged processes and marking only modified processes as unscheduled. The iScheduler agent then iteratively selects an unscheduled process, constructs and solves its subproblem, and commits one local schedule via the learning-based solution-selection module. This procedure continues until the candidate set becomes empty, after which per-process schedules are aggregated into the final schedule $(S_i)_{i \in T'}$ (Algorithm 1).

For training, we adopt a reconfiguration-aware DQN with experience replay (Algorithm 2). At each iteration, the agent applies an ϵ -greedy rule to select a process from the current candidate set, executes one transition (subproblem construction, solution commitment, and state update), and stores the resulting tuple (x_v, P_v, r_v, x_{v+1}) in the replay buffer. The Q-network is optimized by minimizing the mean squared error using a periodically synchronized target network.

4 Experimental Evaluation

This section presents a comprehensive experimental evaluation of iScheduler. We conduct extensive experiments on the proposed L-RIPLIB dataset to answer the following key questions:

- **How does iScheduler perform compared with existing optimization methods?** We compare its large-scale solving quality and runtime against MIP, CP, COpter, and POP (§ 4.2).
- **How effective is the learned scheduling-order strategy?** We evaluate whether iScheduler’s process-selection policy outperforms standard heuristic orders (§ 4.3).
- **How does the proposed solution-selection mechanism influence performance?** We compare the learning-based selection against alternative feasible-schedule selection heuristics (§ 4.3).

4.1 Setup

L-RIPLIB Dataset. We build L-RIPLIB from 30 seed schedules collected from daily scheduling operations on a cloud computing platform. From these seeds, we generate 1,000 instances by varying four drivers: the number of processes n , the number of tasks $|T|$, the number of resources $|\mathcal{R}|$, and the number of precedence constraints $|P|$. Table 1 summarizes the statistics of the seed data.

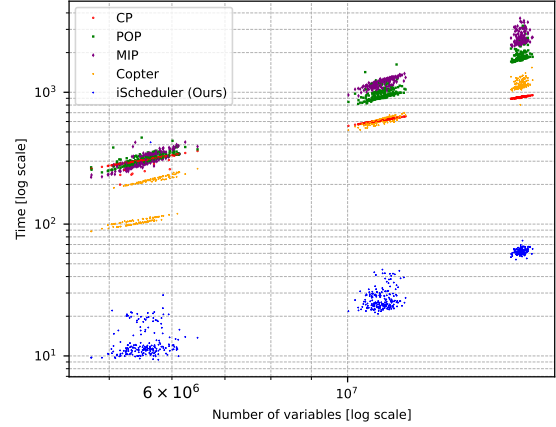


Figure 5: Runtime versus problem size (number of variables, log scale). Each point corresponds to one test instance.

Table 1: Parameter values of the seed data.

Parameters	Values
n	[100, 1000]
$ T $	[1000 – 40000]
$ \mathcal{R} $	{1, 3}
$ P $	[1931, 36010]

Each instance provides (i) the original problem definition q , (ii) an available feasible schedule $(S_i)_{i \in T}$ for q , and (iii) an updated instance q' for reconfiguration. We obtain q' by modifying 5% of task parameters relative to q . We also report the CP-SAT solving time under a fixed nominal cap and the corresponding lower bound for each instance. As shown in Table 2, we stratify instances into *Easy*, *Normal*, and *Hard* based on n , and we list the training/testing split used in our evaluation. Notably, we *intentionally* train iScheduler only on *Easy*; *Normal/Hard* are held out for zero-shot OOD evaluation, which tests whether the learned policy transfers to larger-scale and harder regimes without access to *Normal/Hard* training data. Appendix A gives the full schema and construction details of L-RIPLIB.

Hardware and Environment. All experiments run on a 2-socket AMD EPYC 7763 64-core processor with 512GB of DDR4 memory. We limit solvers (Gurobi 13.0.0 (Gurobi Optimization, LLC 2025) and OR-Tools CP-SAT 9.14 (Periron and Didier 2025)) to 8 threads (no significant speedup is observed beyond 8 threads(Xu et al. 2023)).

Evaluation Metrics. To ensure fairness, all solvers use the same time budget ($\text{Time}_{\text{limit}} = 0.1 \times |T|$ seconds) and identical warm-start conditions when applicable. If a solver fails to find a feasible solution within the budget, we keep the run active until it returns the first feasible schedule and record that time. We evaluate performance using the following metrics:

- **Objective value:** total resource investment cost as defined in Eq. (1).

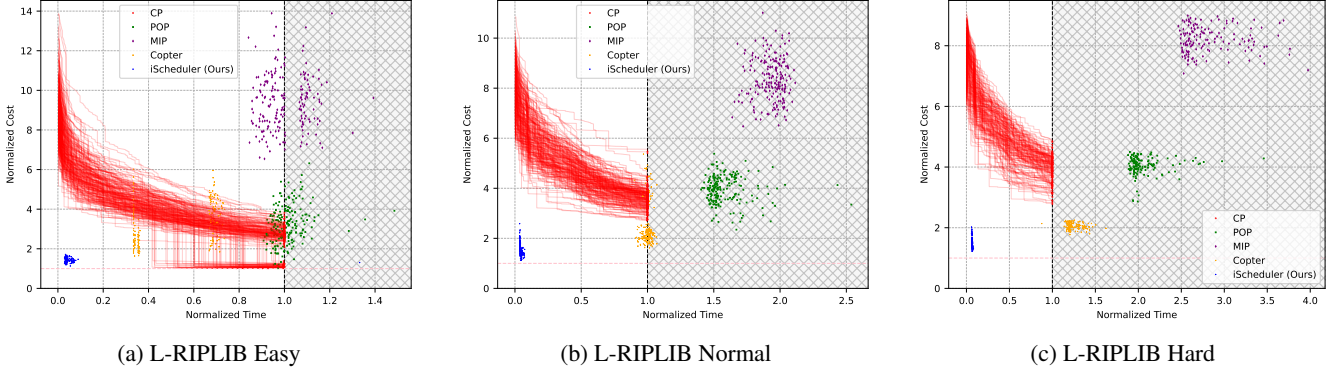


Figure 6: **Cost-time trade-offs on L-RIPLIB.** Subfigures (a)–(c) report the normalized objective Obj/LB versus the normalized runtime $t/Time_{\text{limit}}$ for each instance, where LB is the best-known (time-capped) lower bound (given by OR-Tools CP-SAT) and the horizontal line at $y=1$ indicates the bound. Each marker corresponds to the final solution returned by iScheduler, MIP, COpter, and POP (best solution within the time budget, or the first feasible one if no feasible solution is found within $Time_{\text{limit}}$). Only CP (OR-Tools CP-SAT) additionally plots its anytime improvement trajectory of incumbents over time.

Table 2: Statistics of the L-RIPLIB benchmark.

Category	n	$ T $	Training	Testing
Easy	100	[2634, 3589]	400	200
Normal	200	[5566, 6572]	0	200
Hard	300	[8929, 9509]	0	200

- **Solving time:** wall-clock time to obtain the best solution within the time budget; if no feasible solution is found before $Time_{\text{limit}}$, we report the wall-clock time to the first feasible solution.

Training Details and Hyperparameter Search. We train the reconfiguration-aware DQN agent in Algorithm 2 on the training split of L-RIPLIB (Table 2), using Adam ($lr = 0.001$), replay buffer size $N = 10,000$, minibatch size $k = 128$, $\epsilon = 0.05$, target update frequency $K = 10$. We tune $\alpha \in \{10, 100, 300, 500, 1000\}$ and $\gamma \in \{0, 0.8, 0.9, 0.95, 0.99\}$, selecting $\alpha = 100$, $\gamma = 0.9$. For solution selection, we fix the pool size $m = 2$ to limit enumeration overhead.

4.2 Performance Comparison

We evaluate all methods on L-RIPLIB in the *reconfiguration* setting, where each test case provides an original instance q , an available schedule $(S_i)_{i \in T}$, and an updated instance q' to be rescheduled under changed parameters. We compare iScheduler against four strong baselines: 1) **MIP**: An MIP formulation solved by Gurobi; 2) **CP**: A CP formulation solved using OR-Tools CP-SAT; 3) **COpter** (Subramanya et al. 2025): A Proximal Point Algorithm (PPA) and warm-start-based continual optimization framework solved by Gurobi; 4) **POP** (Narayanan et al. 2021): A partitioned optimization method that splits the RIP into 8 subproblems with equal resources and solves them in parallel with Gurobi.

On large-scale instances (L-RIPLIB Normal/Hard), some

baselines do not return a feasible schedule within the time limit, whereas iScheduler remains stable. Across Easy/Normal/Hard, iScheduler reduces time-to-feasibility by $10.57 \times$ – $43.66 \times$ (Table 3) while preserving competitive solution quality. Figure 5 summarizes the scalability trend: as the problem size (number of variables, in log scale) increases, iScheduler consistently achieves the lowest runtime among all compared methods. Figure 6 further visualizes the cost-time frontier, where iScheduler consistently achieves a stronger balance between objective value and runtime, with the advantage being most pronounced on large and tightly constrained instances.

4.3 Ablation Study

We randomly sample 20 instances from L-RIPLIB Hard and conduct ablations to isolate the impact of key design choices. Unless otherwise stated, all ablated variants share the same decomposition pipeline and subproblem solver; differences arise only from the corresponding selection policy.

Comparison of Scheduling Orders We compare iScheduler’s learned process-selection policy with classical ordering heuristics: 1) **Custom Critical Path Method (CCPM)** (Teichteil-Königsbuch et al. 2023): Orders processes lexicographically by attributes $(LF_{\mathcal{P}}, PT_{\mathcal{P}})$, where $LF_{\mathcal{P}}$ is the latest finish time and $PT_{\mathcal{P}}$ is the total processing time; 2) **Max Resource Requirement Rule (MRRR)** (Regnier-Coudert and Povéda 2021): A greedy heuristic that prioritizes scheduling the unscheduled process with the highest resource requirement in \mathcal{C}_{PL} ; 3) **Dummy (DUM)**: A greedy heuristic that selects the unscheduled process with the largest task set size $|T_{\mathcal{P}}|$; 4) **Random Ordering (RAND)**: Randomly selects a process from \mathcal{C}_{PL} at each iteration. All methods use the same decomposition and subproblem solver, so the only degree of freedom is the selection order.

As reported in Table 4, iScheduler achieves the lowest objective value, reducing the average cost by 8.6–24.4%, while

Table 3: Performance comparison of iScheduler, MIP, CP, COpter, and POP on L-RIPLIB. Lower ObjVal and Time (in seconds) indicate better performance.

Method	L-RIPLIB (Easy)		L-RIPLIB (Normal)		L-RIPLIB (Hard)	
	ObjVal	Time	ObjVal	Time	ObjVal	Time
MIP	11784.5±1810.6	309.65±41.47	20618.9±2218.7	1186.66±84.59	30240.1±1694.3	2597.03±306.21
CP	2775.6±1089.4	304.63±20.73	8809.3±1038.5	613.18±18.25	14401.2±1653.5	919.26±12.05
COpter	4078.2±1356.0	157.38±57.96	6055.1±2015.0	612.87±30.87	7560.0±423.6	1150.01±86.65
POP-8	4024.3±1200.0	311.73±29.97	9751.9±1395.6	974.36±99.90	14957.6±1123.1	1907.02±212.14
iScheduler	1788.0±180.9	14.89±28.73	3762.7±610.0	27.18±5.05	5469.8±613.6	62.11±3.00

Table 4: Performance of different scheduling-order strategies on L-RIPLIB. Lower ObjVal and Time (in seconds) indicate better performance.

Method	ObjVal	Time
CCPM	5006.4±436.9	57.96±4.73
MRRR	5096.5±296.8	59.55±2.71
DUM	6055.4±276.2	57.86±4.12
RAND	5965.7±411.6	57.25±3.25
iScheduler	4576.1±180.4	60.10±4.21

Table 5: Objective value ratio (lower is better) of solution-selection strategies normalized to iScheduler’s learning-based method.

Selection Strategy	ObjVal
MAD	1.12×
TV	1.15×
MCT	1.28×
RAND-LS	1.63×
iScheduler	1.00 ×

incurring only minor overhead (within 5% of the fastest heuristic RAND). These results suggest that the learned policy captures long-range interaction patterns that fixed rules do not exploit.

Comparison of Solution Selection Policies We evaluate the learned ranking-based solution-selection module against representative heuristic policies: moving average of differences (MAD), total variation (TV), minimum completion time (MCT), and random local solution (RAND-LS). Compared with these heuristic selection rules, iScheduler reduces the global cost by 10.7%–38.7% (Table 5). A plausible explanation is that smoothness-oriented metrics (e.g., MAD/TV) reduce local fluctuations but do not adequately account for cross-resource coupling, while MCT tends to commit aggressive early schedules that later restrict feasibility. In contrast, the learned selector better aligns local commitments with downstream global impact.

5 Limitation

Although iScheduler achieves strong empirical performance, three limitations remain.

First, the training cost of the feasible-solution selection

module remains high. The current design evaluates multiple candidate local schedules per iteration and trains a value network with a pairwise ranking objective. Constructing supervision requires completing the remaining scheduling procedure for each candidate to obtain its final cost, which increases the number of solver rollouts and couples high-dimensional states with a large candidate space. Future work will reduce this cost by tightening candidate generation to produce a small set of high-quality candidates, distilling the selector into a lighter architecture, and reusing trajectories with off-policy evaluation to avoid repeated full rollouts.

Second, the current framework lacks a theoretical characterization of performance. iScheduler combines decomposition, RL, and iterative commitment, so it does not provide approximation guarantees or convergence statements for the end-to-end pipeline. A rigorous analysis that relates solution quality to overlap intensity in the process-level graph and to the magnitude of reconfiguration would improve confidence for cost-sensitive deployments.

Third, the current implementation solves subproblems in a serial manner by scheduling one process at a time. Runtime therefore scales with the number of iterations and the cost of each subproblem solve. A parallel variant will solve multiple processes concurrently under controlled conflict resolution and commit compatible decisions in a batch, which reduces wall-clock time on instances with many processes.

6 Conclusion

This paper shows that large-scale RIPs benefit from being solved as a sequence of coupled subproblems rather than as a single monolithic program. We propose iScheduler, which models iterative decomposition as an MDP and learns process-selection policies to navigate long-range interactions induced by shared resources and overlapping time windows. To support realistic evaluation, we introduce L-RIPLIB, an industrial-scale benchmark with 2,500–10,000 tasks per instance. Experiments demonstrate that iScheduler achieves competitive resource costs with substantially lower time-to-feasibility than strong solver baselines at scale. Under dynamic updates, iScheduler reuses unchanged schedules and reschedules only affected processes, which reduces reconfiguration latency while preserving feasibility and solution quality. Overall, these results support a learning-guided continual optimization approach for industrial-sized RIP instances.

References

Achiam, J.; Adler, S.; Agarwal, S.; Ahmad, L.; Akkaya, I.; Aleman, F. L.; Almeida, D.; Altenschmidt, J.; Altman, S.; Anadkat, S.; et al. 2023. GPT-4 Technical Report. *arXiv preprint arXiv:2303.08774*.

Brody, S.; Alon, U.; and Yahav, E. 2021. How attentive are graph attention networks? *arXiv:2105.14491*.

Cai, H.; Bian, Y.; and Liu, L. 2024. Deep reinforcement learning for solving resource constrained project scheduling problems with resource disruptions. *Robotics and Computer-Integrated Manufacturing*, 85: 102628.

Debels, D.; and Vanhoucke, M. 2007. A decomposition-based genetic algorithm for the resource-constrained project-scheduling problem. *Operations Research*, 55(3): 457–469.

Demeulemeester, E.; Vanhoucke, M.; and Herroelen, W. 2003. RanGen: A random network generator for activity-on-the-node networks. *Journal of scheduling*, 6(1): 17–38.

Ding, X.; Zhang, Y.; Chen, B.; Ying, D.; Zhang, T.; Chen, J.; Zhang, L.; Cerpa, A.; and Du, W. 2025. Towards VM Rescheduling Optimization Through Deep Reinforcement Learning. In *Proceedings of the Twentieth European Conference on Computer Systems*, EuroSys '25, 686–701. New York, NY, USA: Association for Computing Machinery. ISBN 9798400711961.

Dubey, A.; Jauhri, A.; Pandey, A.; Kadian, A.; Al-Dahle, A.; Letman, A.; Mathur, A.; Schelten, A.; Yang, A.; Fan, A.; et al. 2024. The Llama 3 Herd of Models. *arXiv preprint arXiv:2407.21783*.

Faiz, A.; Kaneda, S.; Wang, R.; Osi, R. C.; Sharma, P.; Chen, F.; and Jiang, L. 2024. LLMCarbon: Modeling the End-to-End Carbon Footprint of Large Language Models. In *The Twelfth International Conference on Learning Representations*.

Fernandez, J.; Na, C.; Tiwari, V.; Bisk, Y.; Luccioni, S.; and Strubell, E. 2025. Energy Considerations of Large Language Model Inference and Efficiency Optimizations. In Che, W.; Nabende, J.; Shutova, E.; and Pilehvar, M. T., eds., *Proceedings of the 63rd Annual Meeting of the Association for Computational Linguistics (Volume 1: Long Papers)*, 32556–32569. Vienna, Austria: Association for Computational Linguistics. ISBN 979-8-89176-251-0.

Fey, M.; and Lenssen, J. E. 2019. Fast Graph Representation Learning with PyTorch Geometric. In *ICLR Workshop on Representation Learning on Graphs and Manifolds*.

Fireteanu, V.-V. 2020. Agile Methodology Advantages when delivering Internet of Things projects. In *2020 12th International Conference on Electronics, Computers and Artificial Intelligence (ECAI)*, 1–5.

Ganian, R.; Hamm, T.; and Mescoff, G. 2021. The complexity landscape of resource-constrained scheduling. In *Proc. International Joint Conference on Artificial Intelligence (IJCAI)*, 1548–1554.

Gerhards, P. 2020. The multi-mode resource investment problem: a benchmark library and a computational study of lower and upper bounds. *Or spectrum*, 42(4): 901–933.

Gurobi Optimization, LLC. 2025. Gurobi Optimizer Reference Manual.

Kolisch, R.; and Sprecher, A. 1997. PSPLIB-a project scheduling problem library: OR software-ORSEP operations research software exchange program. *European Journal of Operational Research*, 96(1): 205–216.

Kolisch, R.; Sprecher, A.; and Drexl, A. 1995. Characterization and generation of a general class of resource-constrained project scheduling problems. *Management science*, 41(10): 1693–1703.

Kroll, J.; Friboim, S.; and Hemmati, H. 2017. An Empirical Study of Search-Based Task Scheduling in Global Software Development. In *2017 IEEE/ACM 39th International Conference on Software Engineering: Software Engineering in Practice Track (ICSE-SEIP)*, 183–192.

Li, K.; and Willis, R. 1992. An iterative scheduling technique for resource-constrained project scheduling. *European Journal of Operational Research*, 56: 370–379.

Li, X.; Pan, D.; Wang, Y.; and Ruiz, R. 2022. Scheduling multi-tenant cloud workflow tasks with resource reliability. *Science China Information Sciences*, 65(9): 192106.

Liu, D.; Xu, Z.; and Li, F. 2021. A three-stage decomposition algorithm for decentralized multi-project scheduling under uncertainty. *Computers and Industrial Engineering*, 160: 107553.

Liu, X.; Zhao, Y.; Liu, S.; Li, X.; Zhu, Y.; Liu, X.; and Jin, X. 2024. MuxFlow: efficient GPU sharing in production-level clusters with more than 10000 GPUs. *Science China Information Sciences*, 67(12): 222101.

Narayanan, D.; Kazhamiaka, F.; Abuzaid, F.; Kraft, P.; Agrawal, A.; Kandula, S.; Boyd, S.; and Zaharia, M. 2021. Solving large-scale granular resource allocation problems efficiently with pop. In *Proceedings of the ACM SIGOPS 28th Symposium on Operating Systems Principles*, 521–537.

Perron, L.; and Didier, F. 2025. CP-SAT v9.13. https://developers.google.com/optimization/cp/cp_solver/. Accessed: 2025-05-07.

Regnier-Coudert, O.; and Povéda, G. 2021. An empirical evaluation of permutation-based policies for stochastic RCPSP. In *Proc. Genetic and Evolutionary Computation Conference Companion (GECCO)*, 1451–1458.

Si, Z.; Gu, L.; Ju, Y.; Zeng, D.; and Jin, H. 2026. Collaborative multi-granularity distributed registry planning for fast container image pulling. *Frontiers of Computer Science*, 20(10): 2010617.

Song, Z.; Zhang, X.; and Eriksson, C. 2015. Data Center Energy and Cost Saving Evaluation. *Energy Procedia*, 75: 1255–1260. Clean, Efficient and Affordable Energy for a Sustainable Future: The 7th International Conference on Applied Energy (ICAE2015).

Stefan, K.; Andreas, S.; Peter, J. S.; and Jürgen, Z. 2018. Mixed-integer linear programming and constraint programming formulations for solving resource availability cost problems. *European Journal of Operational Research*, 266(2): 472–486.

Strubell, E.; Ganesh, A.; and McCallum, A. 2019. Energy and Policy Considerations for Deep Learning in NLP. In Korhonen, A.; Traum, D.; and Márquez, L., eds., *Proceedings of the 57th Annual Meeting of the Association for Computational Linguistics*, 3645–3650. Florence, Italy: Association for Computational Linguistics.

Subramanya, S. J.; Dennis, D. K.; Smith, V.; and Ganger, G. R. 2025. COpter: Efficient Large-Scale Resource-Allocation via Continual Optimization. In *Proceedings of the ACM SIGOPS 31st Symposium on Operating Systems Principles*, SOSP ’25, 322–340. New York, NY, USA: Association for Computing Machinery. ISBN 9798400718700.

Teichteil-Königsbuch, F.; Povéda, G.; Barba, G. G. d. G.; Luchterhand, T.; and Thiébaux, S. 2023. Fast and robust resource-constrained scheduling with graph neural networks. *Proc. of the Thirty-Third International Conference on Automated Planning and Scheduling (ICAPS)*, 32: 623–633.

Vanhoucke, M.; Coelho, J.; and Batselier, J. 2016. An overview of project data for integrated project management and control. *The Journal of Modern Project Management*, 3(3): 158–158.

Vanhoucke, M.; Coelho, J.; Debels, D.; Maenhout, B.; and Tavares, L. V. 2008. An evaluation of the adequacy of project network generators with systematically sampled networks. *European Journal of Operational Research*, 187(2): 511–524.

Xu, Z.; Yan, F. Y.; Singh, R.; Chiu, J. T.; Rush, A. M.; and Yu, M. 2023. Teal: Learning-Accelerated Optimization of WAN Traffic Engineering. In *Proceedings of the ACM SIGCOMM 2023 Conference*, 378–393.

A L-RIPLIB Dataset

The L-RIPLIB dataset is available through Huggingface (<https://huggingface.co/datasets/YixiangHu/L-RIPLIB>). In L-RIPLIB, each instance is stored in a JSON format, which contains the following key elements:

- Tasks T : The list of task names, representing the various activities to be managed within the instance.
- Earliest_start e : The list of earliest start times for each task, indicating the minimum time at which each task can commence.
- Deadline l : The list of deadlines (latest finish times) for each task.
- Duration d : The list of durations for each task, specifying how long each task is expected to take from start to finish.
- Dependencies P : The list of task dependencies, outlining which tasks must be completed before others can begin, thereby establishing the sequence of execution.
- Resources r : The resources allocated to each task, detailing the specific inputs or tools required for task completion.
- Costs c : The unit cost of each kind of resource;
- Task_start $(S_i)_{i \in T}$: A solution given by CP-SAT within a limited time ($0.1 \times |T|$ seconds).

- Best_cost: The total resource cost corresponding to the solution;
- Time: The time CP-SAT used to solve this instance;
- Bound: A lower bound of total resource cost given by CP-SAT;
- Modified_data Δq : the difference between q and q' .

B Industrial Deployment and Use Cases of iScheduler

The exponential growth of enterprise data and the shift toward data-driven decision-making have made efficient resource scheduling a business-critical capability. Modern data-processing platforms—whether on-premises clusters or third-party clouds—submit thousands of heterogeneous jobs each day, driving highly variable demand for CPU, memory, and I/O resources. Poorly timed job launches create pronounced load spikes, which in turn throttle throughput, delay downstream analytics, and inflate infrastructure costs.

Synapse production deployment. Figure 7 depicts Synapse, a fixed-quota data platform that previously relied on heuristic, expert-driven job calendars. Before iScheduler, roughly half of the 24-hour horizon regularly entered a high-load regime, during which jobs queued, timed out, or even failed, triggering costly re-runs. By replacing manual calendars with iScheduler’s RL-guided iterative planning, Synapse now flattens its CPU-utilization curve, shifting workloads from peak to off-peak windows, achieving \$3.6 M annual savings in compute spend and 120 person-days of orchestration effort eliminated per year.

From a data-center perspective, iScheduler acts as a temporal load-shaping mechanism that performs peak shaving and valley filling: it shifts deferrable workloads away from short-term peaks and improves infrastructure utilization. This matters because a substantial fraction of data-center electricity is associated with power delivery and cooling; empirical evidence reports that cooling alone accounts for about 40% of total data-center energy consumption in certain deployments (Song, Zhang, and Eriksson 2015). In parallel, the rapid scaling of Large Language Model (LLM) (Achiam et al. 2023; Dubey et al. 2024) training and inference introduces increasingly energy-intensive GPU workloads, and recent studies quantify the end-to-end carbon footprint of LLMs and show that inference/efficiency choices materially change total energy use (Faiz et al. 2024; Fernandez et al. 2025; Strubell, Ganesh, and McCallum 2019). Against this backdrop, reducing instantaneous peak power while preserving the required computation lowers the headroom required by power-and-cooling infrastructure and mitigates demand peaks, aligning iScheduler with cost- and sustainability-driven objectives in modern computing centers.

Generalization beyond data pipelines. Because iScheduler optimises arbitrary RIPS rather than a single domain, it transfers seamlessly to other large-scale scheduling contexts, e.g.:

- **Virtual Machine (VM) Rescheduling.** Cloud-scale data centers constantly create and retire VMs, leaving “resource crumbs”—small, unusable CPU and memory

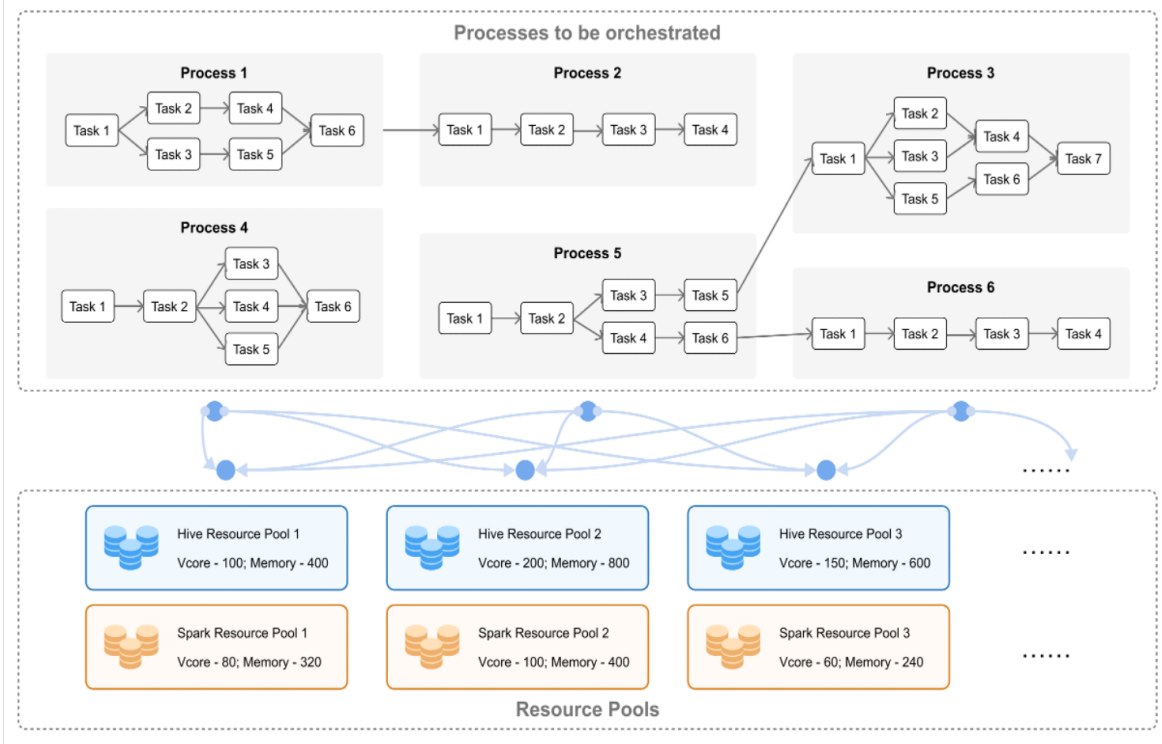


Figure 7: Synapse: Processes to be orchestrated and resource pools.

slices—scattered across physical hosts. Periodic consolidation (i.e., migrating selected VMs to alternate hosts (Ding et al. 2025)) allows idle machines to be powered down, but choosing which VMs to move and in what order is an RIP in its own right. By modelling each live-migration as a task with bandwidth and memory-copy constraints, iScheduler can generate a migration sequence that minimises residual fragmentation.

- **Development-Team Task Scheduling.** Software-company dev teams often work on multiple project versions in parallel, each with distinct workloads and deadlines, while interdependent tasks from different functional units—UI, testing, and core development—must be coordinated (Fireteanu 2020; Kroll, Friboim, and Hemmati 2017). Viewed as a complex RIP, this scenario can also be tackled by iScheduler: its iterative solving strategy produces a practical shift plan that guides the team’s day-to-day scheduling.

C Symbols and Definitions

The symbols we used in this paper and corresponding definitions are listed in Table 6.

Table 6: Symbols and Definitions.

Symbol	Definition
T	Set of tasks in a Resource Investment Problem (RIP) instance.
\mathcal{R}	Set of renewable resource types.
P	Set of precedence constraints, $P \subseteq T \times T$.
t	Discrete time index in the scheduling horizon.
n	Number of unscheduled processes after decomposition.
q	An RIP instance (task set, resources, precedence, demands, costs, durations, earliest starts, deadlines).
d_i	Duration (processing time) of task i .
$r_{i,k}$	Demand of task i for resource k during its execution.
c_k	Cost of provisioning one unit of resource k .
R_k	Provisioned capacity (amount) of resource k for the whole project.
e_i	Earliest start time of task i .
l_i	Deadline (latest completion bound) of task i (used via $S_i \leq l_i - d_i$).
S_i	Scheduled start time of task i .
$\mathcal{U}(S, t)$	Set of tasks active at time t under schedule S .
$G_T = (T, P)$	Task-level directed acyclic graph (DAG): nodes are tasks; edges are precedence constraints.
\mathcal{P}_i	A process (task subset) obtained by grouping tasks via weakly connected components of G_T .
$T_{\mathcal{P}_i}$	Set of tasks belonging to process \mathcal{P}_i .
$G_{PL} = (V_{PL}, E_{PL})$	Process-level interaction graph; nodes are processes; edges represent process interactions.
v	Iteration index of the iterative scheduling procedure.
\mathcal{P}_v	Process selected by the agent at iteration v to schedule next.
RPU	Resource Pool Usage profile induced by already scheduled processes.
$u_k(t)$	Current usage of resource k at time t from already committed (scheduled) processes.
RIP_v	Subproblem constructed at iteration v for the selected process \mathcal{P}_v given the current committed schedule/usage.
$R_k^{(v)}$	Global provisioned capacity of resource k after iteration v (used in subproblem constraints together with $u_k(t)$).
\mathcal{C}_{PL}	Candidate set of unscheduled processes in G_{PL} .
m	Solution pool size (number of candidate local schedules generated per subproblem for solution selection).
α	Positive scaling factor used in the terminal reward.
ES_P	Earliest start of a process: $ES_P = \min_{i \in T_P} e_i$.
LF_P	Latest finish bound of a process: $LF_P = \max_{i \in T_P} l_i$.
$t_{\text{start}}, t_{\text{end}}$	Overlap window bounds for an edge (P_i, P_j) : $t_{\text{start}} = \max(ES_{P_i}, ES_{P_j})$, $t_{\text{end}} = \min(LF_{P_i}, LF_{P_j})$.